Langmuir
Article
pubs.acs.org/Langmuir

Influence of Mechanical Properties of Nanoparticles on Macrocrack Formation

Ludovic Pauchard,*,† Bérengère Abou,‡ and Ken Sekimoto‡,§

†Laboratoire Fluides, Automatique et Systèmes Thermiques, Université Paris VI, Paris XI, UMR CNRS 7608, France, ‡Laboratoire Matière et Systèmes Complexes, UMR 7057 CNRS & Université Paris Diderot, France, and §Gulliver, UMR7083 CNRS & ESPCI, France

Received January 13, 2009. Revised Manuscript Received March 23, 2009

We present an experimental investigation of drying suspensions of both hard and soft nanolatex spheres. The crack formation is examined as a function of the proportion of hard and soft deformable particles, leading to tunable elastic properties of the drying film. In our experimental systems, no crack formation could be observed below an onset value of the proportion in hard spheres $\phi \sim 0.45$. During the drying process, the mass of films with various compositions in hard and soft spheres is measured as a function of time. The results suggest that the soft particles undergo deformation that releases the internal stresses.

Introduction

The use of coatings in most applications is based on the formation of a continuous film during drying. The industrial applications of these films depend on their final mechanical properties, but the film formation is a complex process and is considered as a succession of several steps such as concentration of dispersion, particle packing, particle deformation, and so on. During consolidation, cracking and warping may generally need to be avoided. The phenomenon of cracking in drying films depends on several parameters.[1,2] Some of them control the boundary conditions of the film: degree of adhesion to the substrate and the rate of evaporation controlled by the ambient temperature and humidity. Others are due to the film itself: film thickness, particle size, and mechanical properties of the close packed array of particles.[3−5]

In this Article, we suggest a model system to study and quantify the crack patterns observed in brittle or soft consolidated systems such as paint layers. It consists of a drying film of dispersed hard and soft spheres in controlled proportions. The influence of the mechanical properties of the film on the final crack patterns is investigated. As a latex film dries, it is transformed from a colloidal dispersion into either a close packed array of particles or a continuous polymer film, with both having mechanical integrity. The drying curves (mass and drying rate) are recorded as a function of time. The nature of the latex film obtained at the end of the drying process depends on the glass transition temperature of the particles and the ambient temperature. If the glass transition temperature of the latex particles is higher than the ambient temperature (hard particles), the final film is found to contain a large number of cracks. Contrarily (soft particles), the final film may be homogeneous.[6] We measure the crack spacing as a function for various compositions in hard and soft spheres.

It has been believed that, when the film is applied on a glass substrate, evaporation of the solvent concentrates the particles into a close packed array before the film cracks to release the stresses. Our measurement of the mass and the crack spacing shows, however, that the evaporation from the surface of the film is possibly blocked in the presence of soft particles and that, even in the case of solely hard spheres, there is more interparticle space than in the close packed state upon appearance of the first crack.

Materials and Methods

The experiment consists of a drying dispersion of binary mixtures of particles. In this way, two different types of particles are considered: hard ones and deformable ones. Hard particles are made of a styrene copolymer and acrylic acid. The particles are polydisperse enough not to crystallize. Deformable particles are made of a copolymer of styrene and carboxylated butadiene. The particle concentration is determined by weighing after drying the suspensions. The colloidal spheres, provided by Rhodia Recherche (Aubervilliers, France), with two different glass transition temperatures T_g, are 30 nm in diameter. At room temperature, this allows us to work with hard spheres (T_g = 100 °C) and soft spheres (T_g = 0 °C), the last that can deform more easily than hard spheres. The glass transition temperatures were estimated from the particle core composition.

The initial volume fraction of both dispersions is $\phi_0 = 0.3$, and the densities of pure dry material of hard and soft spheres are, respectively, $\rho_h = 1.08 \pm 0.02$ g/cm^3 and $\rho_s = 1.10 \pm 0.02$ g/cm^3. The proportion ϕ in hard spheres is defined as $\phi = V_h/(V_h + V_s)$, where $V_{h(s)}$ is the volume of hard (respectively soft) spheres. Binary mixtures are magnetically stirred during 15 min at room temperature and then sonicated at a 1 s on/off pulse interval during 300 s. The suspensions are stable without solvent loss. Drying experiments are conducted at room temperature and relative humidity around RH = 37 ± 2%. In our experiments, the transfer of water in air is limited by diffusion and therefore controlled by the relative humidity. The surface tension of each suspension is measured by the Wilhelmy plate method and displays a nearly identical value of 57 ± 5 mN/m .

A circular container (diameter ∼ 16 mm, height ∼ 0.5 mm) is filled by the dispersion. The bottom of the container is a carefully

*Corresponding author. E-mail: pauchard@fast.u-psud.fr.

(1) Brinker, C. J.; Scherer, G. W. *Sol-Gel Science*; Academic Press: New York, 1990; pp 453−488.
(2) Atkinson, A.; Guppy, R. M. *J. Mater. Sci.* **1991**, *26*, 3869.
(3) Groisman, A.; Kaplan, E. *Europhys. Lett.* **1994**, *25*, 415.
(4) Martinez, C.; Lewis, J. *Langmuir* **2002**, *18*, 4689–4698.
(5) Qamar, N.; Rharbi, Y. *Macromolecules* **2008**, *41*(15), 5928.
(6) *Film Formation in waterborne coatings*; Provder, T., Winnik, M., Urban, M., Eds.; ACS Symposium Series 648; American Chemical Society: Washington, DC, 1996.Spiro, J. S.; Farinha, J. P. S.; Winnik, M. A. *Macromolecules* **2003**, *36*, 7791.

cleaned glass substrate, and the lateral walls are Altuglas (Figure 1). The contact line of the dispersion remains quenched at the upper edge of the container during the drying process. We obtain a film of approximately constant thickness in the center of the container, that is, about 70% of the total surface area, and avoid the anisotropy due to large evaporation at the borders. Starting from the beginning of the drying process, the mass of the container filled with the suspension is measured with a precision balance (Sartorius). The mass, $m(t)$, of films with different compositions in hard and soft spheres is recorded during the drying process. The drying rate, $|dm/dt|$, is then extracted from the mass measurements. Simultaneously, the crack morphology is recorded with a Leica camera positioned on the top of the sample. At the end of the drying process, a film with a thickness H is obtained. Final film thickness is measured by successively focusing a microscope objective on both the substrate and film surface (the accuracy on the measurement is 2 μm).

The macroscopic elastic response of the colloidal gel is characterized using the CSM Instruments microindentation testing (MHT) by measuring the penetration depth of an indenter tip driven into the sample by applying force. The volume fraction of the solvent $\phi_w(t)$ at time t is deduced from the measurement of the sample mass $m(t)$, assuming that (1) only the solvent evaporates from the sample, (2) no air penetrates into the sample up to time t (see ref 7), and (3) the volumes occupied by hard and soft particles are constant throughout the drying process (even in case of deformation of spheres). At time t, the sample mass $m(t)$ simply is $m(t) = \rho_w V_w(t) + \rho_h V_h + \rho_s V_s$, where $\rho_{w(h,s)}$ is the density of water (respectively hard and soft spheres) and $V_{w(h,s)}$ the volume occupied by water (respectively hard and soft spheres). Given a mixing ratio ϕ, the volumes, $V_{(h,s)}$, occupied by hard and soft spheres can easily be calculated from the known quantities $m(0)$, $V_{tot}(0)$, proportion of hard spheres ϕ, and initial volume fraction ϕ_0. The solvent volume fraction $\phi_w(t) = V_w(t)/V_{tot}(t)$ can then be expressed implicitly as the solution of the mass balance equation:

$$\phi_w(t) = \frac{1}{V_{tot}(t)}\left[\frac{m(t)}{\rho_w} - V_h\frac{\rho_h}{\rho_w} - V_s\frac{\rho_s}{\rho_w}\right] \quad (1)$$

and volume balance equation, $(1-\phi_w(t))V_{tot}(t) = \rho_h V_h + \rho_s V_s$.

Note that, under assumption (2) and in the case where the particles are not deformed from the spherical shape, the value $\phi_w(t)$ should be smaller than $1 - \phi_{rcp}$, where ϕ_{rcp} (≈ 0.64) is the random close packing volume fraction.

Results

Figure 2 shows the drying curves, mass m, and drying rate $|dm/dt|$ of suspensions as a function of the dimensionless time, t/t_D, where $t_D = H_0/v_e$ denotes the characteristic drying time (H_0 is the initial layer thickness and v_e is the evaporation rate of water in the air, typically 10^{-4} mm/s at RH = 40%). This dimensionless time allows us to balance for the slight differences in relative humidity between the curves.

In the particular case of a pure suspension of hard spheres ($\phi = 1$), the drying rate change with time has been separated into three periods, to which physical processes have been usually associated.[1,8,9] During the first regime associated with the existence of a continuous liquid network through the sample, the solvent evaporates at a constant rate from the free surface (region I in the inset in Figure 2). Then the particles are dynamically arrested. The resulting close packed array of particles, saturated with solvent, is under compression at its free surface due to high capillary pressure. However, this shrinkage is limited by the adhesion on the solid substrate which limits the contraction of the gel. This frustration causes mechanical tensions that build up with time. The constant rate drying period is followed by a nonlinear drying rate period where the drying rate decreases (regime II). The free water still evaporates from the surface where the liquid is carried from the inside by the fluid flow. During this stage, the particles' mechanical properties are of importance, since the particles may deform elastically under high capillary pressure and thus close the interparticles voids. During the final regime (III), at some point the liquid phase breaks up into separate fractions and the drying process is usually said to enter the second "falling rate period", completing the drying process. The associated drying rate is much slower than those of the two first regimes.

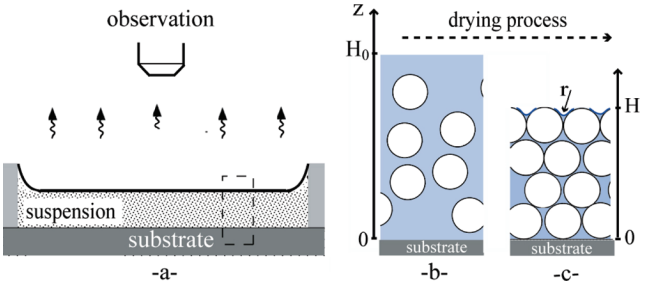

Figure 1. (a) Experimental setup (side view). The suspension is deposited in a circular container which is 16 mm in diameter. Reproducible adhesion of the film on the substrate (glass slide) is obtained by carefully cleaning of the glass slide. Evaporation of the solvent from the surface induces consolidation of the film. The top of the sample was recorded during the whole drying process through a Leica microscope. The region shown in the dashed rectangle is sketched in (b,c). Illustration of the film of initial thickness H_0 just after the film deposition (b) and when a close packed array of particles saturated by solvent is formed (c). The curvature, r^{-1}, of the air−solvent meniscus increases during evaporation.

In the case of mixtures of hard and soft spheres, these three regimes can be identified as well, as can be seen in Figure 2 ($\phi \neq 1$). Besides, the drying process is found also to strongly depend on the film composition in both hard and soft spheres. During the first stage, the evaporation rate remains independent of the film composition. However, in the presence of soft spheres ($\phi \neq 1$), slower evaporation of the solvent could be measured during regime II. The more the film contains soft spheres, the slower the evaporation is, as clearly shown in Figure 2. At the end of the measurements, the final mass of the films containing soft spheres is larger than in the case of hard sphere films. Because hard and soft spheres have same diameter and density, these results suggest that water remains trapped in the films containing soft spheres. Consequently, this strongly suggests that, during the film drying, soft particles can deform, causing the interparticle voids to close and block further evaporation. The more soft particles in the suspension, the more interparticle voids can be closed by soft particles deformation, resulting in earlier stopping of evaporation with increasing soft sphere proportion.[10]

Moreover, for ϕ high enough ($\phi > 0.45$ in our experimental conditions), the stress buildup results in crack formation. The experiments show that cracks start invading the film in the beginning of regime II (inset in Figure 2). Measurements of the time-lag cracking, t_{crack}, at which cracking occurs are shown in

(7) Dufresne, E. R.; Corwin, E. I.; Greenblatt, N. A.; Ashmore, J.; Wang, D. Y.; Dinsmore, A. D.; Cheng, J. X.; Xie, X. S.; Hutchinson, J. W.; Weitz, D. A. *Phys. Rev. Lett.* **2003**, *91*, 224501.
(8) Coussot, P. *Eur. Phys. J.* **2000**, *15*, 557–566.
(9) Ghosal, S.; Emami-Naeini, A.; Harn, Y. P.; Draskovich, B. S.; Pollinger, J. P. *J. Am. Ceram. Soc.* **1999**, *82*, 513–520.

(10) Similar blockage of evaporation has recently reported in the drying experiments of polymer gel. Huraux, K. Ph.D. Thesis, Paris University VI, France, 2008. Huraux, K.; et al. *Macromolecules*, submitted for publication.

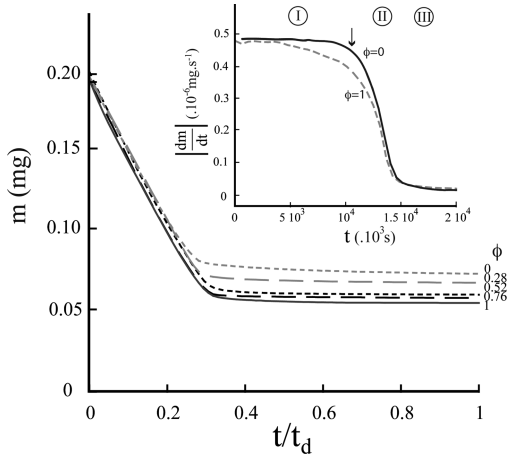

Figure 2. Mass of drying films as a function of the dimensionless time for various compositions in hard and soft spheres. From top to bottom, the proportion in hard spheres is 0, 0.28, 0.52, 0.76, and 1. Inset: drying rate curves for films composed with hard ($\phi = 1$) and soft ($\phi = 0$) spheres. The arrow indicates the time of crack formation for the film of pure hard spheres. The drying process of colloidal films can be subdivided into three regimes: the first one, denoted by I, is known as the constant rate period characterized by a constant evaporation rate; in region II, the drying rate starts to decrease; and finally, in the falling rate period, denoted by III, the liquid phase breaks up into separate fractions.

Table 1. As can be seen, the more the film contains soft spheres, the more delayed cracking occurs. An estimate of the water volume fraction upon the first appearance of cracks, $\phi_{w,crack} \equiv \phi_w(t_{crack})$, can be deduced from eq 1 taking into account the total mass of the sample at $t = t_{crack}$ measured from the mass variations with time (Figure 2). The solid volume fraction, $1 - \phi_{w,crack}$, can then easily be deduced from the data. The value $\phi_{w,crack}$ decreases with decreasing proportion of hard spheres ϕ (Table 1). The maximum value $(\phi_{w,crack})_{max} = 0.40 \pm 0.03$ (when cracking occurs) is obtained when the film is purely composed of hard spheres. Experiments show that cracking occurs earlier in time for hard films, and in this case the volume fraction of water reaches a maximum value. In the case of a relatively soft film ($\phi = 0.52$), $\phi_{w,crack} = 0.30 \pm 0.03$ is smaller than $1 - \phi_{rcp} = 0.36$, which suggests that some of the interparticle voids in the film are closed if the assumption (2) mentioned above remains valid. This indicates therefore that some of the soft particles are deformed from their spherical shape.

Figure 3 presents the results obtained for films with a final thickness $H = 170 \pm 5\ \mu$m. At the end of the drying process, the mean cell area is measured as a function of the film composition ϕ in hard and soft spheres. Below a threshold value in hard spheres, $\phi \sim 0.45$, no crack formation can be observed and the film remains homogeneous in the horizontal directions. Just above $\phi \sim 0.45$, cracks nucleate in the sample. The cracks' growth stops shortly after their initiation, leading to isolated crack segments. They are either open ended single cracks or starlike patterns with three cracks at 120° from each other and centered at defects as nucleation sites.[11] At higher proportion in hard spheres ϕ, cracks may propagate in the sample, connecting each other and dividing the film into adjacent cells of the surface area denoted by A_{cell}; this quantity will be the parameter of interest in the following, because it can be accurately measured from observations.[12] In Figure 3, the characteristic crack spacing is found to decrease with the proportion in hard spheres ϕ. This suggests that more crack generation is needed to relax the mechanical stresses in the film with increasing ϕ (Figure 3, $\phi \sim 0.58$, 0.70, and 1).

Table 1. Time T_{crack} at Which Cracking Occurs for Gel of Various Compositions ϕ[a]

ϕ	t_{crack}(s) (±300 s)	$\phi_{w,crack}$ (±0.03)
0.52	11 373	0.30
0.76	10 863	0.33
0.87	10 685	0.37
1	10 353	0.40

[a] An estimate of the water volume fraction $\phi_{w,crack}$ when cracking occurs is also calculated. The solid volume fraction $1 - \phi_{w,crack}$ can then easily be deduced from the data.

Moreover, in the range of ϕ corresponding to crack formation, residual stresses in the polygonal cells can induce another mode of crack formation. When the stored elastic strain energy in the film overcomes the adhesion energy on the substrate film, the detachment due to crack formation at the interface takes place between the film and the substrate. Consequently, this process releases in-plane stresses in both in-plane directions. The buckle propagation stops when the elastic strain energy is just overcome by the adhesion energy. As a result, a single adhering region is located in each polygonal cell at the final stage of the process. In the case of films of pure hard particles, the adhering region is preferentially circular at the final stage of the process[13] (region bordered by dashed line inside the polygonal cell in Figure 4). Changing the composition of the film, different morphologies can be observed. At the final stage of the detachment process, the pattern of the adhering region can be characterized by the relative variation of the respective surface area, A_{adh}, also the relative variation of the circularity, C_{adh}, describing the relative change between the perimeter of the adhering area and the polygonal cell area (Figure 4) (note that a circularity value of 1 indicates a perfect circle whereas a value approaching 0 indicates an increasingly elongated polygon). The ratio between the adhering surface area and the polygonal surface area decreases when increasing the composition in soft particles in the film: the buckle propagation is more difficult. Moreover, for a composition of hard particles approaching 0.6, detachment of the film is simply located close to the crack opening (Figure 4).

Discussion

Let us first recall a widely accepted macroscopic picture of the mechanism of cracking induced by desiccation.[14] A colloidal gel film of infinite horizontal dimensions and of initial thickness given by the dot-dashed horizontal line is dried down to the thickness shown by a filled thick rectangle (Figure 5a). The material cannot change its dimensions along its horizontal directions because the gel is attached to the substrate. If it were detached, the relaxed state of the dried gel material would have the form represented by the dashed open rectangle in Figure 5a or the two dashed open rectangles in Figure 5b *if* we cut the material into two blocks. The gel attached to the substrate in Figure 5a is, therefore, under horizontal stretching as a whole (to compensate the substrate is under lateral compression).

In Figure 5b, a crack opens by creating the V-shaped new surface. The tensile deformation of the gel material is partially relaxed within a distance comparable to the thickness. This reduces the stored elastic energy. The formation of one crack is favored if this gain of elastic energy overcompensates the cost of creating the crack surfaces. Thus cracks appear successively.

(11) Toga, K. B.; Alaca, B. E. *Phys. Rev. E* **2006**, *74*, 021405.
(12) Bohn, S.; Pauchard, L.; Couder, Y. *Phys. Rev. E* **2005**, *71*, 046214.
(13) Pauchard, L. *Europhys. Lett.* **2006**, *74*, 188–194.
(14) Routh, A. F.; Russel, W. B. *Langmuir* **1999**, *15*, 7762–7773.

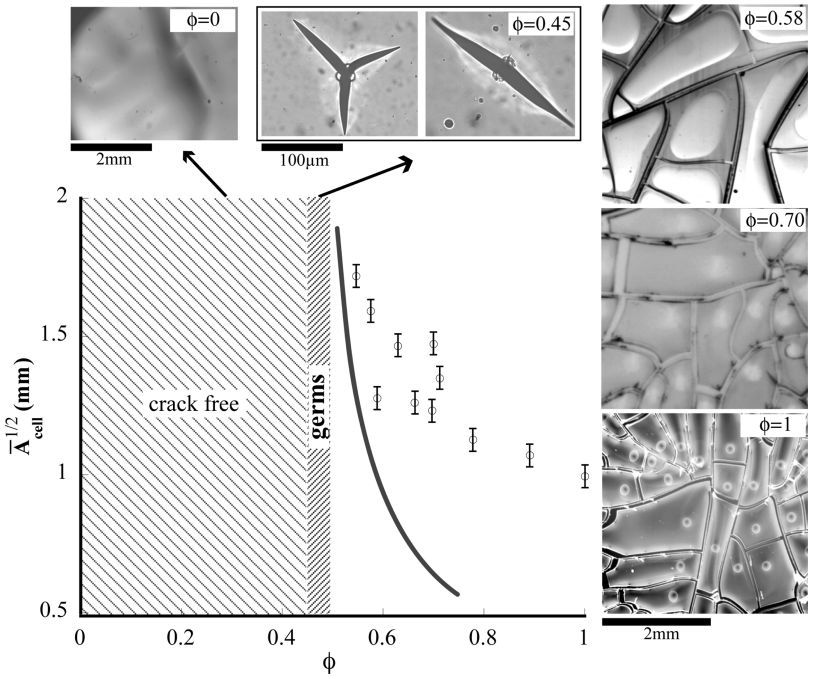

Figure 3. Crack patterns quantification versus film composition. The square root of the mean cell area, $\overline{A}_{cell}{}^{1/2}$, is plotted as a function of the proportion in hard spheres ϕ for a final film thickness $H = 170 \pm 5\ \mu$m. Below a critical value of hard spheres $\phi \sim 0.45$, no crack formation could be observed. Around $\phi \sim 0.45$, isolated cracks form in the drying film. At higher volume fraction, crack formation takes place and divides the structure into polygonal adjacent cells. Images of crack patterns for $\phi = 0.58, 0.70, 1$ are shown at the final stage of the drying process: bright regions inside each polygonal cell correspond to the adhering region at the final stage of the delamination process. The drying process was investigated at RH = 37%. The dark line corresponds to the theoretical adjustment.

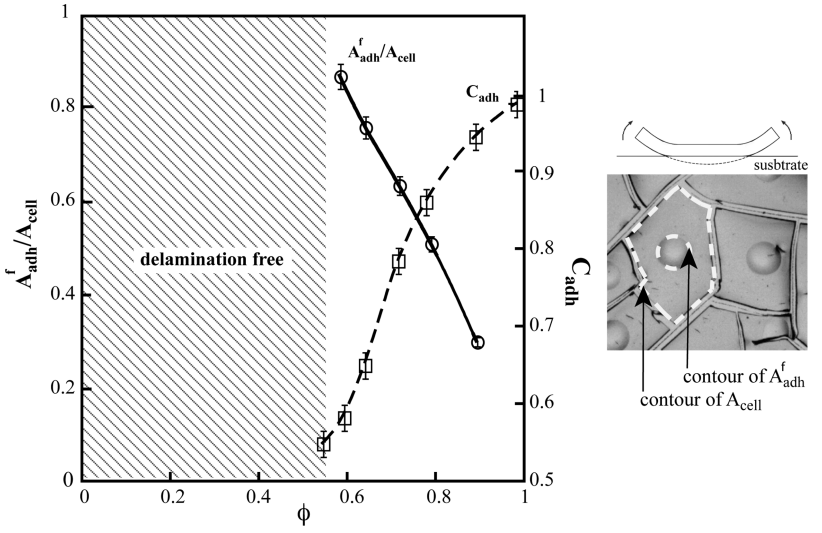

Figure 4. Comparison of the buckle morphologies for different proportions in hard spheres, ϕ, at the final stage of the delamination process. (○) Measurements of the final dimensionless *adhering* surface area, A^f_{adh}/A_{cell}, versus the proportion in hard spheres, ϕ. (□) Measurements of the final circularity, C_{adh}, versus the proportion in hard spheres, ϕ (C_{adh} is defined as 4π(area)/(perimeter)^2, with area and perimeter being measured on a given surface area). Lines are guides for the eyes.

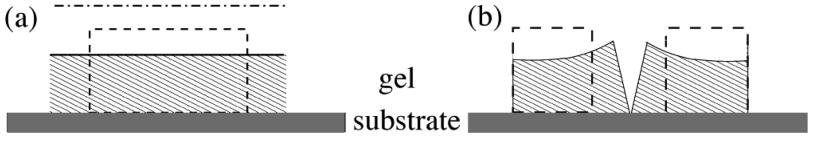

Figure 5. Schematic sectional view of the film. (a) The initial sample (up to the dot-dashed horizontal line) is dried down to the thickness shown by a filled thick rectangle: the material cannot change its dimensions along the horizontal directions because the gel is attached to the substrate. If the gel were not attached to the substrate, it would take the form of the dashed open rectangle. (b) Cutting the material into two blocks: a crack opens by creating the V-shaped new surface when the gel is attached to the substrate. If the gel were not attached to the substrate, it would take the form of the dashed open rectangle.

If, however, a new crack were to appear at too small distance from pre-existing ones, the released elastic energy would be not enough to compensate the cost of the surface energy of the crack. In this scenario, the final crack spacing is determined according to Russel et al.[15]

Recently, there are different models that predict how the elastic properties of the particles influence the creation of cracks upon drying. Man and Russel[16] showed that, for a given film thickness, the gel with hard particles has less tendency to create cracks than in the case of soft particles. The physical reason is that the network of hard particles can store little elastic energy before the capillary (under-)pressure reaches its maximum value. Beyond this limit, the air penetrates into individual interparticle space without creating a macroscopic crack. When we compare their results with our experiments, the latter show apparently the opposite tendency about the elasticity. The discrepancy will be ascribed to the inhomogeneity of the drying film,[10] while the setup of Man and Russel[16] controlled the pressure to maintain quasi-equilibrium. Singh and Tirumkudulu[17] proposed an alternative case of soft particles and predicted that the crack creation is unfavorable for the colloidal dispersions of very soft particles. They argued that, upon drying, the stocked elastic energy is bounded from above if the deformed particles fill the entire space of gel. Both scenarios predict that the crack is easier to be created in thicker films, in accordance with experiments. However, the minimum thickness for the crack creation, H_c, is predicted to increase with the shear elastic modulus of the particle G for hard particles and to decrease with G for soft particles. Moreover, we note that the argument on the crack spacing by Russel et al.[15] applies to both scenarios.

The crack spacing of mixed colloidal spheres can be predicted along this line (Russel et al.[15]) if we suppose that, from a macroscopic point of view, our suspension is a homogeneous material with a tunable rigidity. This rigidity can be quantified by the measurement of the macroscopic elastic response as a function of the fraction of hard particles, ϕ (Figure 6 and Appendix). In our experiments, the film of a fixed thickness develops cracks only when the hard particles occupy a minimum volume fraction. Therefore, our system behaves more like the colloidal suspension of soft particles discussed by Singh and Tirumkudulu.[17] However, if we look into more quantitative aspects, the threshold value of the elastic coefficient, $\overline{G} \equiv \overline{G}^*$, for the appearance of the first crack is larger by 6−7 orders of magnitude than what one can deduce from their paper (eq 2 therein). Perhaps this can be attributed to the fact that the soft particles of ref 18 are still elastic, that is, well below the glass transition temperature, while the soft particles used here deform viscously and do not store elastic energy. The theoretical prediction of the crack spacing, W versus $\overline{G}$, with appropriate nondimensionalization (Tirumkudulu and Russel[18]) can be compared with our measurement of the crack spacing, $A_{cell}^{1/2}$, as a function of ϕ (Figure 3) indirectly if we use our simple superposition approximation of $\overline{G}$ as a function of ϕ. The theory predicts the divergence of the spacing to thickness ratio as

$$\frac{W(\phi)}{H} \approx \ln\left(\frac{2\overline{G}^*}{\overline{G}(\phi) - \overline{G}^*}\right) \qquad (2)$$

for $\overline{G}$ slightly above $\overline{G}^*$. The predicted W/H (the solid curve for $\phi > 0.45$ in Figure 3), however, depends on ϕ much stronger than the measured data.

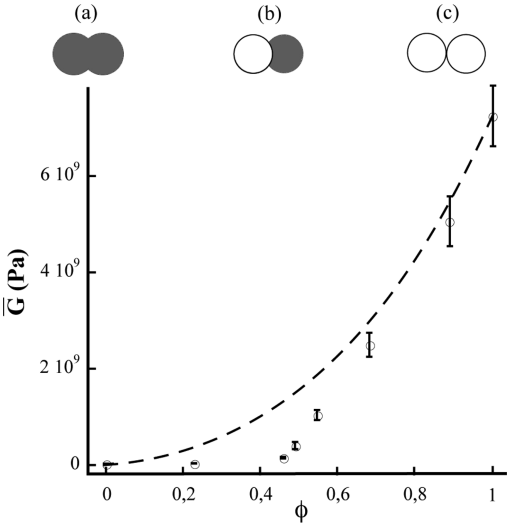

Figure 6. Macroscopic elastic response of the solid film as a function of the proportion in hard spheres. Dots represent the measurements performed with microindentation testing, while the dashed line corresponds to the model, adapted from Russel et al.[15] to the case of mixtures of hard and soft spheres.

At the moment, we have no concise theory to explain these discrepancies. However, we note several differences between our experiments and the assumptions for the models mentioned above. First, our measurement exhibits the blocking of evaporation if the sample contains a lot of soft particles. We, therefore, should take into account the non-quasistatic effects, especially the inhomogeneity of the solvent content along the vertical direction.[19] Second, the packing of particles may not be close to the random close packing. In accordance with Table 1, the fracture appears earliest with purely hard particles, and upon the appearance of the first fracture the purely hard particles occupy the least fraction of volume ($1 - 0.40 = 0.60$). While this fraction less than ϕ_{rcp} is rather surprising in view of the hypothesis of random close packing in the previous papers, it is consistent with our observation that the sample's linear dimension continues to shrink slowly by typically ~10% after the appearance of cracks. In other words, the *volumetric plasticity* may also be a factor limiting the stored elastic energy.

Conclusion

In this work, we have investigated drying kinetics and crack patterns in gels of different compositions. Whereas the first regime of drying kinetics is not influenced by the composition of the film, evaporation from the film surface is blocked in the presence of soft particles. This first result suggests a closing of the interparticle voids during the gel consolidation. In this hypothesis, the process is driven by internal modifications of the film, that is, soft particles deformation, releasing a part of the elastic energy. The existence of a hard particle volume fraction is underlined at the onset of cracking for our physicochemical system; this value depends on the glass transition temperature of the soft component, since viscous deformation relieves the stress and depends on the drying conditions. As a result, the number of cracks decreases with the proportion in soft spheres. The poor quantitative agreement with simple extrapolation on existing theoretical models suggests that the nonequilibrium blockade of evaporation as well as the

(15) Russel, W. B.; Wu, N.; Man, W. *Langmuir* **2008**, *24*, 1721–1730.
(16) Man, W.; Russel, W. B. *Phys. Rev. Lett.* **2008**, *100*, 198302.
(17) Singh, K. B.; Tirumkudulu, M. S. *Phys. Rev. Lett.* **2007**, *98*, 218302.
(18) Tirumkudulu, M. S.; Russel, W. B. *Langmuir* **2005**, *21*, 4938–4948.
(19) Johnson, K. L. *Contact Mechanics*; Cambridge University Press: 1985; section 4.1.

volumetric plastic compaction toward the close packing play an important role for films containing soft particles.

Acknowledgment. This work was supported by the ANR Programme JC-JC ANR-05-JCJC-0029 "Morphologies". We would like to thank L. Limat for useful discussions and I. Jeté-Côté for the help in the experiments. K.S. acknowledges the discussion with T. Narita and F. Lequeux.

Appendix: Linear Superposition Approximation of the Elastic Response of a Colloidal Gel

Russel et al.[15] proposed a mean-field approach for the elastic response of a dense packing of spherical particles. They assumed the affine deformation of each pair of contacting particles and average over all orientations of contact surface. They showed that, under the uniform compaction normal to the substrate, by a factor $(1 - \varepsilon_0)$, that is, under the strain $\varepsilon \equiv -\varepsilon_0 \hat{z}\hat{z}$ (with $\hat{z}$ being the unit vector normal to the substrate), the stress exerted by the particle network, σ_0, is given by

$$\sigma_0 = -p_0\delta - \frac{\overline{G}}{6}[\delta + 3\hat{z}\hat{z}]{\varepsilon_0}^{3/2}$$

where δ is the unit matrix, and the hydrostatic compression p_0 is the capillary pressure in the case considered. The parameter $\overline{G}$ is defined as

$$\overline{G} \equiv \frac{\phi_p N}{\pi} \frac{G}{2(1-\nu)}$$

where G and ν are, respectively, the Young modulus and the Poisson ratio of the particles and N ($\approx$6) and ϕ_p, respectively, are the mean number of contacts for a given particle and the volume fraction of the particles in the random packing state. As a straightforward generalization of this approach for the mixture of hard and soft particles, we can replace $G/(1 - \nu)$ by the average over the values for the different types of contacts, that is, the hard−hard, hard−soft, and soft−soft pairs. For the hard−hard and soft−soft pairs, we take the values of $G/(1- \nu)$ of the hard particles, $G_h/(1 - \nu_h)$, and soft particles, $G_s/(1 - \nu_s)$, respectively.

For the hard−soft pairs, we must replace the above $G/(1 - \nu)$ by the harmonic average (Johnson[19]), that is

$$\left[G/(1-\nu)\right]^{-1} \rightarrow \left(\left[G_h/(1-\nu_h)\right]^{-1} + \left[G_s/(1-\nu_s)\right]^{-1}\right)/2$$

The macroscopic elastic response $\overline{G}$ is then obtained when replacing $G/(1 - \nu)$ by the average over the three types of contacts, such as

$$\begin{aligned} G/(1-\nu) \rightarrow\ & \phi^2 G_h/(1-\nu_h) \\ & + 4\phi(1-\phi)\left(\left[G_h/(1-\nu_h)\right]^{-1} + \left[G_s/(1-\nu_s)\right]^{-1}\right)^{-1} \\ & + (1-\phi)^2 G_s/(1-\nu_s) \end{aligned}$$

where ϕ is the proportion of hard particles among all particles. From this expression, it can easily be shown that the presence of soft spheres decreases the value of the effective modulus. In accordance with Russel et al.,[15] the smaller effective modulus $\overline{G}$, the smaller stored elastic energy in the film.

Using these modifications, the theoretical macroscopic uniaxial modulus, $\overline{G}$, is plotted as a function of ϕ in Figure 6 (dashed curve), where we used the values, $G_h = 10^4$ MPa, $G_s = 30$ MPa, and $\nu_h = \nu_s = 1/3$. Figure 6 also shows the macroscopic elastic response $\overline{G}$ measurements for various compositions in hard and soft spheres ϕ, performed by microindentation tests.

For ϕ below about 30%, both the experiment and theory show that the magnitude of the macroscopic modulus is mostly determined by that of soft particles. However, the measurement exhibits a clear onset phenomena at around 40% from which the macroscopic modulus rises sharply. The latter behavior suggests the percolation of rigidity in the mixture of soft and hard particles.